Collision-less Magnetic Reconnection

Induced by Chaotic Motion of Particles

(   )

by

96587
Ryusuke NUMATA

Department of Quantum Engineering and Systems Science,
Faculty of Engineering,
University of Tokyo

February, 2001

Directed by

Professor	Zensho YOSHIDA
Professor	Yuichi OGAWA
Associate Professor	Haruhiko HIMURA

A thesis
Submitted to the Division of Engineering,
the Graduate School of the University of Tokyo,
as the Partial Fulfillment for the Requirements
of the Degree of Master of Engineering

Acknowledgments

Abstract

Charged particle chaos and its collective effect in a magnetic reconnection like field is investigated numerically. We propose Y-shaped model field to describe magnetic reconnection and study the behavior of charged particles in the microscopic point of view. The existence of at least one positive Lyapunov exponents shows that the motion of the particles is chaotic. Then, we switch to the way of statistical mechanics to investigate macroscopic properties of the chaotic motion of the particles. Collective of particles is accelerated in average affected by the electric field perpendicular to the magnetic field in weak magnetic field region. The finite average velocity in the direction of electric field means the existence of effective resistivity even in a collision-less regime. The effective resistivity due to the effective collision induced by chaotic motion is estimated. Ohmic heating by this effective resistivity is also shown. The effective collision induced by the collective of particles which behave like chaotic is essentially a different mechanism from classical collision.

Contents

List of Figures

v

List of Tables

Chapter 1

Introduction

The concept of chaos was first introduced to the science to study the planetary motion. It was realized to be essentially impossible to solve analytically the dynamics of more than three celestial bodies with mutual interactions by the gravitational force. H. Poincaré suggested the importance of an qualitative analysis of the dynamics, such as to study the reason or the geometrical property of the complex orbit. Recent years, the concept of chaos become one of the main theme of science and applied to various fields. Plasma physics also contributed to the chaos theory. The structures of the magnetic fields in toroidal plasma confinement vessels or the dynamics of the charged particles in electromagnetic fields may become chaotic. The purpose of this thesis is to explain the production of anomalous resistivity in a magnetic reconnection phenomena by applying the chaotic theory to the dynamics of charged particles.

Magnetic reconnection [1][2][3] is important phenomena because of its connection with the topology of field lines. In general, a change of topology means a change of equilibrium, and a release of magnetically stored energy. It occurs in so many different contexts. Examples are: solar flares, the magnetosphere of the earth, dynamo theories of the origin and evolution of fields in stars, accretion disks and galaxies, and laboratory, and fusion plasmas.

Magnetic reconnection concerns the breaking and mending of magnetic field lines. Because the resistance is low and inductance is large in high temperature plasmas, the decay time of field is long and any magnetic field changes very slowly. If the plasma resistivity was zero, the lines of force would indeed be embedded in the plasma, and would follow the plasma displacements to preserve the number of lines and their topology. However, there are conceivable motions that crush the lines together leading to such large current densities that even for a very small resistivity a line can cease following the plasma

and can break and change its topology. Such intense current layers are the seat of magnetic reconnection. In these layers a line can break in two and its ends become attached to other lines that are also breaking. The whole process is conveniently called magnetic reconnection. Such topological change corresponds to a change from one equilibrium state to another. Since the two states may have different magnetic energies, this transfer between equilibrium corresponds to a conversion of magnetic energy to other forms of energy, such as kinetic or thermal energy. If the energies of two equilibria are greatly different, then a large amount of energy is released.

The main problem of the magnetic reconnection is that we can not explain fast energy release rate. Various reconnection models are suggested to explain this fast reconnection rate. The first quantitative model of magnetic reconnection was proposed by Sweet and Parker separately. Sweet-Parker reconnection requires long current sheets and is a rather slow process. The model introduced by Petschek is also important [4]. He noted that considering the effect of slow mode magnetohydrodynamic (MHD) shock on the dissipation region greatly increases reconnection rate. However, it is at present not clear that Petschek reconnection can evolve in natural systems. These theories both treat by the way of MHD and refer to the collisional regime with at least a small resistivity. However, in high temperature rarefied plasmas, such resistivity do not exist a priori. Hence, the MHD approach becomes invalid, and one should switch to a kinetic approach[5] [6]. Also charged particle motion in a reconnection like magnetic field is investigated widely [7] [8] [9]. We consider the stochasticity of the charged particle motion can be an effective mechanism for collisionless anomalous resistivity and lead the fast energy release.

The charged particle chaos in a simple nonuniform one dimensional magnetic field with null points and radio-frequency electric field has been investi-

gated. In such a field, charged particle describes a meandering orbit and the mixing effect of chaos yields a rapid production of kinetic entropy. Although this process saturates a short time, unceasing heating occur by introducing the cascade mechanism toward the collision region. The effective resistivity enhanced by the mixing effect of chaos has been estimated [10]. This nonlinear process can be applied to plasma production that meets the increasing demand for a low-gas-pressure plasma source suitable for use in ultrafine etching of semiconductors[11].

In this thesis, we propose Y-shaped magnetic field to model a reconnection process and study the dynamics of charged particle motion in such a field. The complexity of the field brings about the chaotic motion of particle. Furthermore, because of its geometrical properties, the system becomes open to a flow of particles, and then an exchange of energy from field to the particles steadily occurs. First, we investigate the microscopic behavior of the particles and show that is chaotic. There is still broad gap between the microscopic behavior and the macroscopic quantity. Only statistical analysis gives us informations about the macroscopic property of the system. Thus, we borrow the way of statistics and estimate the macroscopic quantities like temperature, current and resistivity to what the microscopic chaos brings about.

Chapter 2

Model Equation

2.1 Two Dimensional Y-Shaped Model

We propose two dimensional Y-shaped magnetic field configuration to study charged particle dynamics in a magnetic reconnection like field, that is,

$$\boldsymbol{B} = \begin{pmatrix} b_x y \\ B_y(x) \\ 0 \end{pmatrix} \tag{2.1}$$

where $B_y(x)$ is

$$B_y(x) = \begin{cases} b_y(x - L_x) & (x > L_x) \\ 0 & (|x| \le L_x) \\ b_y(x + L_x) & (x < -L_x). \end{cases} \tag{2.2}$$

The stream line of this model magnetic field with $L_x = 2$ and $b_x = b_y$ is shown in Fig. 2.1. Magnetic field is null at the region where $|x| < L_x$ and $y = 0$, so this plane is called neutral sheet. In the vicinity of the magnetic null sheet (hatched region), magnetic field is so weak that particles are not magnetized and they behave like chaotic. Conversion of magnetic energy to the kinetic energy of the plasma occurs in this domain, so we can refer it as the dissipation region. For steady reconnection, we also have a uniform electric field in $-z$ direction, $\boldsymbol{E} = -E_0 \boldsymbol{e}_z$. Potentials which describe the field are represent as

$$A_z(x, y) = \begin{cases} \frac{1}{2}b_y y^2 - \frac{1}{2}b_x(x - L_x)^2 & (x > L_x) \\ \frac{1}{2}b_y y^2 & (|x| \le L_x) \\ \frac{1}{2}b_y y^2 - \frac{1}{2}b_x(x + L_x)^2 & (x < -L_x) \end{cases} \tag{2.3}$$

$$\phi(z) = E_0 z. \tag{2.4}$$

Here, we mention the characteristic of this configuration. First, this configuration is similar to Harris-type configuration which is often employed to discuss the magnetic reconnection. Harris-type configuration is an equilibrium

solution of the Vlasov-Maxwell equations which represented as

$$B \propto \tanh(\frac{x}{L}) \tag{2.5}$$

where L is the global scale length. A minutes derivation and discussion about Harris configuration is given in Appendix A. In the case that x is much smaller than L, hyperbolic tangent of x is approximated by x, so that $B \propto x/L$. We consider this model configuration as a simplified Harris-type one in the vicinity of the neutral sheet. The second characteristic is the complexity of the field. Because magnetic field depends on x and y, the symmetry of a Hamiltonian of particle in this system is broken. So, the motion of the particle can be chaotic. This is discussed in detail in Sec. 3.1. Finally, in this system, $\boldsymbol{E} \times \boldsymbol{B}$ drift provides plasma inflow to the dissipation region along the y axis and outflow along the x axis. This effect and geometrical property such as bifurcation of the magnetic field make this an open system. In the dissipation region, the flow is violated because of the magnetic null and particles experience the stochastic mixing.

2.2 Normalization

We consider the Newton's equation of motion in the given field,

$$m\frac{d\boldsymbol{v}}{dt} = q(\boldsymbol{E} + \boldsymbol{v} \times \boldsymbol{B}), \tag{2.6}$$

and normalize it by the parameters defined in Table 2.1. The relation between the normalizing parameters are given by

$$B_0 = b_x L_y \tag{2.7}$$

$$T_0 = 1/\frac{|q|B_0}{m} = \frac{m}{|q|B_0}. \tag{2.8}$$

Table 2.1: Normalizing Parameters.

Coordinate	L_y	Global length scale of the system
Magnetic field	B_0	Magnitude of the field at $y = L_y$
Time	T_0	Reciprocal of the cyclotron frequency at $y = L_y$

Thus, we obtain normalized equation of motion

$$\frac{d\hat{\boldsymbol{v}}}{d\hat{t}} = \pm(\frac{|q|T_0^2}{mL_y}\boldsymbol{E} + \hat{\boldsymbol{v}} \times \hat{\boldsymbol{B}}). \tag{2.9}$$

where + and - stand for an ion and an electron, respectively, and hat above the variables denote that they are normalized quantities. Then, we define the parameter describe the intensity of the electric field,

$$\alpha \equiv \frac{|q|T_0^2}{mL_y} = \frac{m}{|q|L_yB_0^2}E_0. \tag{2.10}$$

By substituting the field given in by Eqs. (2.1) and (2.2) into Eq. (2.9), we finally obtain the normalized equations for an electron,

$$\begin{cases} \dot{\hat{v}}_x &= \hat{v}_z\hat{B}_y \\ \dot{\hat{v}}_y &= -\hat{v}_z\hat{y} \\ \dot{\hat{v}}_z &= \alpha - \hat{v}_x\hat{B}_y + \hat{v}_y\hat{y}, \end{cases} \tag{2.11}$$

where

$$\hat{B}_y(\hat{x}) = \begin{cases} \beta(\hat{x} - \gamma) & (\hat{x} > \gamma) \\ 0 & (|\hat{x}| < \gamma) \\ \beta(\hat{x} + \gamma) & (\hat{x} < -\gamma). \end{cases} \tag{2.12}$$

$\beta \equiv b_y/b_x$ is the ratio of the gradient of the magnetic field, $\gamma \equiv L_x/L_y$ is the ratio of the scale of x direction to y direction. Parameters α and γ are the controll parameters, while β is fixed to unity through all simulation discussed in Chapter 4. At the limit $\gamma \to \infty$, the magnetic field is considered to be

8

one dimensional field. A particle motion in such a field is discussed in section 3.1. The relation between the normalized and the real value is summarized in Table 2.2.

Table 2.2: Relation between normalized and real values.

$\hat{x} = 1$	10^{-2} m
$\hat{B}_0 = 1$	10^{-2} T
$\hat{T}_0 = 1$	5.7×10^{-10} s
$\alpha = 1$	1.8×10^5 V/m

Typical values of magnetic field and the scale length of the dissipation region in various situations are given in Table 2.3.

Table 2.3: Typical values of scale length and magnetic filed in observed magnetic reconnection processes.

	Scale Length [m]	Typical Magnetic Field [G]
Solar Corona	10^8	10
Magnetosphere	6.4×10^6	0.31
Galactic Disks	$10^{18} - 10^{20}$	5×10^{-6}
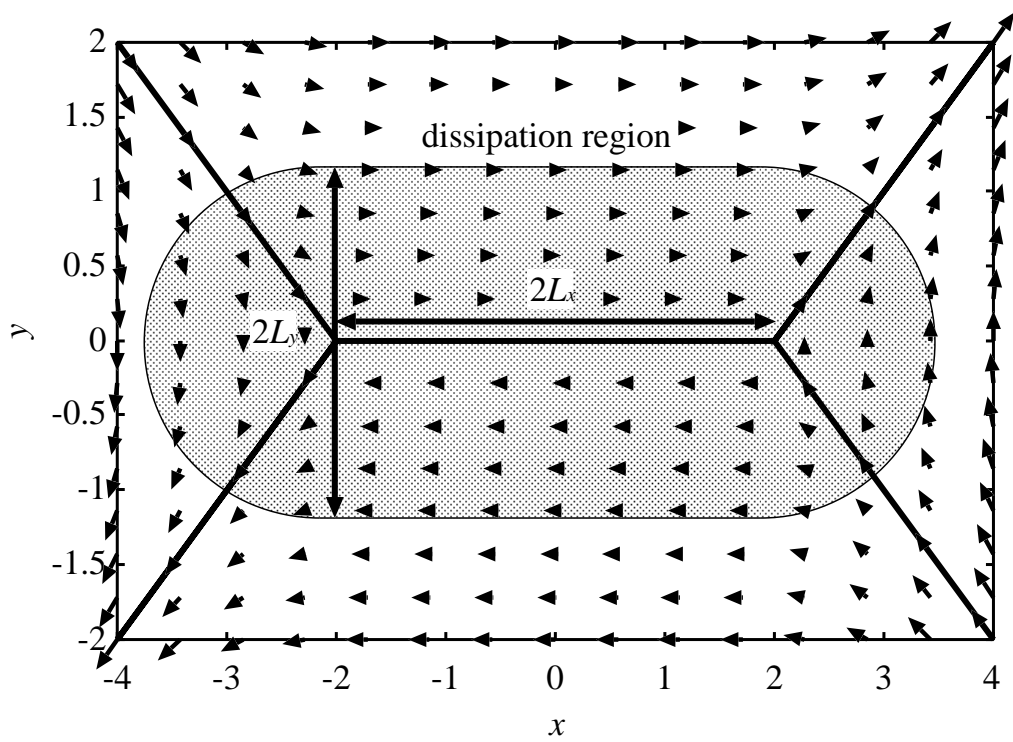
Figure 2.1: Schematic drawing of Y-shaped magnetic field.

Chapter 3

Method for Analyzing the Chaotic System

3.1 Integrability of Charged Particle Motion in Electromagnetic Field

The dynamics of a charged particle in an electromagnetic field can be described by the Hamilton's equation of motion,

$$\frac{d}{dt}\begin{pmatrix} \boldsymbol{x} \\ \boldsymbol{p} \end{pmatrix} = \begin{pmatrix} \frac{\partial H}{\partial \boldsymbol{p}} \\ -\frac{\partial H}{\partial \boldsymbol{x}} \end{pmatrix}, \tag{3.1}$$

where H is a Hamiltonian which is generally a function of coordinate $\boldsymbol{x}$, momentum $\boldsymbol{p}$ and time t,

$$H(\boldsymbol{x}, \boldsymbol{p}, t) = \frac{(\boldsymbol{p} - q\boldsymbol{A}(\boldsymbol{x}, t))}{2m} + q\phi(\boldsymbol{x}, t). \tag{3.2}$$

$\boldsymbol{A}$ and ϕ are magnetic potential and electrostatic potential, respectively, m is mass and q is charge of the particle. In the case that the dynamics can be represented by $2N$ dimensional Hamiltonian flow, we can switch to some coordinate system in which the stream line is reduced to the straight line by performing a certain canonical transformation if and only if there exist N constants of motion [12] [13]. Constants of motion α must be in involution, i.e., their Poison brackets with each other must be zero:

$$\{\alpha_i, \alpha_j\} = \sum_k [\frac{\partial \alpha_i}{\partial x_k}\frac{\partial \alpha_j}{\partial p_k} - \frac{\partial \alpha_i}{\partial p_k}\frac{\partial \alpha_j}{\partial x_k}] = 0. \tag{3.3}$$

One can easily find the constants of motion if the dynamics is described by a Hamiltonian form. When the Hamiltonian is independent of a variable, conjugate of the variable is a constant of motion.

Here, we show some examples of integrability analysis of a charged particle dynamics in general electromagnetic fields. We consider the motion in a straight reversed magnetic field, $\boldsymbol{B} = B'x\boldsymbol{e}_z$ (Fig. 3.1). For the magnetic field generated by the vector potential $A_y = \frac{B'}{2}x^2$, the Hamiltonian is given by

$$H(x, p_x, p_y, p_z) = \frac{p_x^2}{2m} + \frac{p_z^2}{2m} + \frac{(p_y - \frac{qB'}{2}x^2)^2}{2m} \tag{3.4}$$

which immediately gives three constants of motions, H, p_y, p_z, then, this system is integrable. If we define the effective potential V_{eff} and new Hamiltonian H' by

$$V_{\text{eff}} = \frac{(p_y - \frac{qB'}{2}x^2)^2}{2m} \tag{3.5}$$

$$H' = H - \frac{p_z^2}{2m} = \frac{p_x^2}{2m} + V_{\text{eff}}, \tag{3.6}$$

the problem is reduced to one dimensional quadrature in the effective potential. The effective potentials and the phase space diagrams in x-p_x plane is shown in Figs. 3.2 and 3.3.

It is important to study the application of electric fields transverse to the magnetic field or a normal component of magnetic fields. These components can break the conservation of constants of motion and then the system may become chaotic. First, we consider a time independent electric field transverse to the magnetic field, $\boldsymbol{E} = E_y \boldsymbol{e}_y$. The effective potential changes to be

$$V_{\text{eff}} = \frac{(p_y - \frac{qB'}{2}x^2 + E_y t)^2}{2m}. \tag{3.7}$$

This gives the description that the potential well in Fig. 3.2 moves with constant $\boldsymbol{E} \times \boldsymbol{B}$ drift velocity. The equation of motion becomes

$$\frac{d^2 x}{dt^2} = -\frac{qB'}{m}(p_x + \frac{qB'}{2}x^2 + E_y t)x. \tag{3.8}$$

The limiting case of $t \to \infty$, the equation is approximated by the equation

$$\frac{d^2 x}{dt^2} \sim xt. \tag{3.9}$$

The Airy function can be satisfied this equation, hence this system is still integrable.

It is proved that time dependent inductive electric field can lead the onset of chaos and the irreversible heating [14] [15]. The application of normal

component of magnetic fields and the onset of chaos is also studied in detail by many researchers [16-22]. The configuration that we proposed also has a normal magnetic field component which can lead the onset of chaos.

3.2 Lyapunov Exponents

Lyapunov exponents play an important role in the theory of both Hamiltonian and dissipative dynamical systems. They provide a computable, quantitative measure of the degree of stochasticity for a trajectory. In addition, there is a close link between Lyapunov exponents and other measures of randomness such as the Kolmogorov entropy and the fractal dimension.

Roughly speaking, the Lyapunov exponents of a given trajectory characterize the mean exponential rate of divergence of trajectories surrounding it.

The theory of Lyapunov exponents was applied to characterize stochastic trajectories by Oseledec. The connection between Lyapunov exponents and exponential divergence was given by Benettin *et al.* and by Pesin, who also established the connection to Kolmogorov entropy. The procedure for computing the Lyapunov exponents was developed by Benettin *et al.* . Here, we give the properties of the Lyapunov exponents.

We define the Lyapunov exponents for the flow $\boldsymbol{x}(t)$ generated by the smooth vector field $\boldsymbol{v}$ in N dimensional phase space

$$\frac{d\boldsymbol{x}}{dt} = \boldsymbol{v}(\boldsymbol{x}(t), t) \tag{3.10}$$

Consider a trajectory and a nearby trajectory with initial condition $\boldsymbol{x}_0$ and $\boldsymbol{x}_0 + \delta\boldsymbol{x}_0$. The time evolution for $\delta\boldsymbol{x}$ is found by linearizing Eq. (3.10) to obtain

$$\frac{d\delta\boldsymbol{x}}{dt} = \boldsymbol{M}(\boldsymbol{x}(t)) \cdot \delta\boldsymbol{x} \tag{3.11}$$

where

$$\boldsymbol{M} = \frac{\partial \boldsymbol{v}}{\partial \boldsymbol{x}} \tag{3.12}$$

is the Jacobian matrix of $\boldsymbol{v}$. We now introduce the mean exponential rate of divergence of two initially close trajectories,

$$\lambda(\boldsymbol{x}_0, \delta \boldsymbol{x}) = \lim_{t \to \infty} \frac{1}{t} \ln \frac{d(\boldsymbol{x}_0, t)}{d(\boldsymbol{x}_0, 0)} \tag{3.13}$$

where $d(\cdot, \cdot)$ is some metric for the phase space, for example, an Eucledian norm. There is an N dimensional basis $\{\hat{e}_i\}$ of $\delta \boldsymbol{x}$ such that for any $\delta \boldsymbol{x}$, λ takes one of the N values

$$\lambda_i(\boldsymbol{x}_0) = \lambda(\boldsymbol{x}_0, \hat{e}_i), \tag{3.14}$$

which are the Lyapunov characteristic exponents. The Lyapunov exponents are related to the evolution of an infinitesimal N dimensional sphere in the phase space (Fig. 3.4). The sphere whose principal axis is defined by $\{\hat{\boldsymbol{e}}_i\}$ will be deformed into an ellipsoid. The Lyapunov exponents can be ordered by size,

$$\lambda_1 \geq \lambda_2 \geq \cdots \geq \lambda_N. \tag{3.15}$$

λ_1 is called the maximum Lyapunov exponent. In the case $\lambda_1 > 0$, initially nearby trajectories diverge exponentially at $t \to \infty$. However, because the volume of the sphere conserves according to the Liouville theorem, they do not diverge in all the directions. If the sphere is expanded in some direction, it must be shrunk in the other directions.

The approach for determining the Lyapunov exponents from a set of differential equations has been developed [23]. The algorithms for the Lyapunov exponents from time series have been also presented .

There are two difficulties in calculating the Lyapunov exponents. Even in the linearized system, the principal axis vectors diverge in magnitude. It is one

problem but can be easily avoided. The other problem is that the direction of each principal axis changes at every moment and each vector falls along the local direction of most rapid growth.

These two problems are overcome by the iterative use of the Gram-Schmidt reorthonormalization (GSR) procedure. Let the initial condition at $t = t_k$ for linearized equation (3.11) be $\{\delta \boldsymbol{x}_1(t_k), \delta \boldsymbol{x}_2(t_k), \cdots, \delta \boldsymbol{x}_N(t_k)\}$, which is a set of orthonormal vectors spanning the surface of an infinitesimal sphere. The set of vectors evolves to $\{\delta \boldsymbol{x}'_1(t_{k+1}), \delta \boldsymbol{x}'_2(t_{k+1}), \cdots, \delta \boldsymbol{x}'_N(t_{k+1})\}$ after $t_{k+1} - t_k$. The set of evolved vectors does not take the form of a sphere but something like ellipsoid. Before the modification of the infinitesimal phase space does not become too extreme, we use the GSR procedure. After the reorthonormalization, the set of vectors is replaced with a new set of orthonormal vectors:

$$
\begin{aligned}
\delta \boldsymbol{x}_1 &= \frac{\delta \boldsymbol{x}'_1}{|\delta \boldsymbol{x}'_1|} \\
\delta \boldsymbol{x}_2 &= \frac{\delta \boldsymbol{x}'_2 - (\delta \boldsymbol{x}'_2 \cdot \delta \boldsymbol{x}_1) \delta \boldsymbol{x}_1}{|\delta \boldsymbol{x}'_2 - (\delta \boldsymbol{x}'_2 \cdot \delta \boldsymbol{x}_1) \delta \boldsymbol{x}_1|} \\
&\cdots \\
&\cdots \\
\delta \boldsymbol{x}_N &= \frac{\delta \boldsymbol{x}'_N - (\delta \boldsymbol{x}'_N \cdot \delta \boldsymbol{x}_{N-1}) \delta \boldsymbol{x}_{N-1} - \cdots - (\delta \boldsymbol{x}'_N \cdot \delta \boldsymbol{x}_1) \delta \boldsymbol{x}_1}{|\delta \boldsymbol{x}'_N - (\delta \boldsymbol{x}'_N \cdot \delta \boldsymbol{x}_{N-1}) \delta \boldsymbol{x}_{N-1} - \cdots - (\delta \boldsymbol{x}'_N \cdot \delta \boldsymbol{x}_1) \delta \boldsymbol{x}_1|}
\end{aligned}
\tag{3.16}
$$

where the time t_{k+1} is omitted from all vectors in equations. Because each vector $\delta \boldsymbol{x}'_1$ tends to point to the direction of most rapid growth, and because the direction of the first vectors is not affected by the GSR procedure, this vector seeks out the most rapidly growing direction after many replacements. Similarly, the space spanned by the first and second vectors tends to lie on the two dimensional space that is most rapidly growing. Hence the second vector seeks out the direction of the second most rapid growth. Thus we can define

the i-th Lyapunov exponents as

$$\lambda_i = \lim_{M \to \infty} \frac{1}{t_M - t_0} \sum_{k=0}^{M-1} \ln \frac{|\delta \boldsymbol{x}_i'(t_{k+1})|}{|\delta \boldsymbol{x}_i(t_k)|} \tag{3.17}$$

where t_k is the time of the k-th replacement step. The Lyapunov exponents obtained from the GSR procedure are then ordered from largest to smallest.

As discussed above, i-th Lyapunov exponent is a growth rate of the i-th most rapidly growing principal axis. Consequently, the sum of the Lyapunov exponents provides a time derivative of the volume of an infinitesimal phase space. Dynamical systems are divided broadly into two groups; one is a dissipative system and the other is a conservative system. While the sum of the Lyapunov exponents reduces in dissipative systems, it is preserved in conservative systems. For example, autonomous Hamiltonian system is given by

$$\frac{d}{dt} \begin{pmatrix} \boldsymbol{q} \\ \boldsymbol{p} \end{pmatrix} = \begin{pmatrix} \frac{\partial H}{\partial \boldsymbol{p}} \\ -\frac{\partial H}{\partial \boldsymbol{q}} \end{pmatrix} \tag{3.18}$$

Here, we measure the rate of change of the volume V from Lie derivative

$$\frac{1}{V} \frac{dV}{dt} = \frac{\partial \dot{\boldsymbol{q}}}{\partial \boldsymbol{q}} + \frac{\partial \dot{\boldsymbol{p}}}{\partial \boldsymbol{p}} = 0. \tag{3.19}$$

The Lyapunov spectrum, the set of Lyapunov exponents, is a useful diagnostics to characterize complicated systems. It may be improper to describe them only with the Lyapunov spectrum. Unpredictable chaos, however, is reflected in the systems that contain at least one positive Lyapunov exponents.

3.3 Statistical Description of the System

In a chaotic dynamical system, it is meaningless to study the precise microscopic state because even an infinitesimal error increases exponentially with time. To find adequate global features to characterize the behavior of the system, we switch to the way of statistical mechanics [24-27].

The basic idea of statistical mechanics is that the system may be replaced with a suitably chosen ensemble of systems, all having the same equations of motion but different initial conditions. The structure of the ensemble is specified by a density function $\rho(x)$ such that $\rho(x)dx$ is the number of sample systems whose initial microstate lies in the volume element dx. This substitution of an ensemble for a single system has the effect of turning x into a stochastic variable X. The range of X consists of all possible microstate and the probability density is, apart from normalization, equal to ρ;

$$P_X(x) = \frac{\rho(x)}{\int \rho(x')dx'} \tag{3.20}$$

Once this basic idea has been accepted it only remains to pick the appropriate P_X.

In statistical mechanics, we suppose that the weight is proportional to the volume of the portion of phase space for a stationary statistical ensemble. This is a fundamental principle of statistical mechanics, which is called the principle of equal probability or a priori probability, as well as the principle that the time-average is the same as the ensemble-average (ergodic hypothesis), and supported by the Liouville theorem. The Liouville theorem says that in the phase space the points representing the dynamical states of an ensemble of identical systems move like particles of an incompressible fluid, that means their point density remains unchanged. We can derive the canonical distribution for a give average energy E by maximizing the entropy with the principle of a priori probability. In a thermal equilibrium with average energy E, the canonical distribution becomes

$$P_i = \exp[-\beta E_i]. \tag{3.21}$$

Here, $T = 1/k_B\beta$ is identified with absolute temperature, k_B is the Boltzmann constant. Once, the canonical distribution is realized, we can construct

18

thermodynamic quantities.

On the other hand, we can construct Gaussian distribution by the central limit theorem. Let $X_1, X_2, \cdots, X_N$ be a set of N independent stochastic variables, each having the same Gaussian probability density $P_X(x)$ with zero average and variance σ^2. Their sum Y has the probability density

$$P_Y(y) = \frac{1}{\sqrt{2\pi N\sigma^2}} \exp\left[-\frac{y^2}{2N\sigma^2}\right]. \tag{3.22}$$

Thus $< Y^2 > = N\sigma^2$ grows linearly with N. On the other hand, the distribution of the arithmetic mean of the variable X becomes narrower with increasing N,

$$\left\langle \left(\frac{X_1 + X_2 + \cdots + X_N}{N}\right)^2 \right\rangle = \frac{\sigma^2}{N}. \tag{3.23}$$

It is therefore useful to define a suitably scaled sum

$$Z = \frac{X_1 + X_2 + \cdots + X_N}{\sqrt{N}}, \tag{3.24}$$

It has a variance σ^2 and hence

$$P_Z(z) = \frac{1}{\sqrt{2\pi\sigma^2}} \exp\left[-\frac{z^2}{2\sigma^2}\right]. \tag{3.25}$$

The central limit theorem states that, even when $P_X(x)$ is not Gaussian, but some other distribution with zero average and finite variance σ^2, Eq. (3.25) is still true in the limit $N \to \infty$.

Once, we chose an appropriate distribution $P(x)$, we define the ensemble average of quantity A

$$\bar{A} = \frac{\int A(x)P(x)dx}{\int P(x)dx}. \tag{3.26}$$

In a chaotic system, we can not assume that the principle of a priori distribution is realized. So, we must study the distribution of stochastic variables by direct numerical simulation. If the Gaussian distribution is constructed, we consider the priciple of a priori distribution is realized and define ensemble average by the distribution.
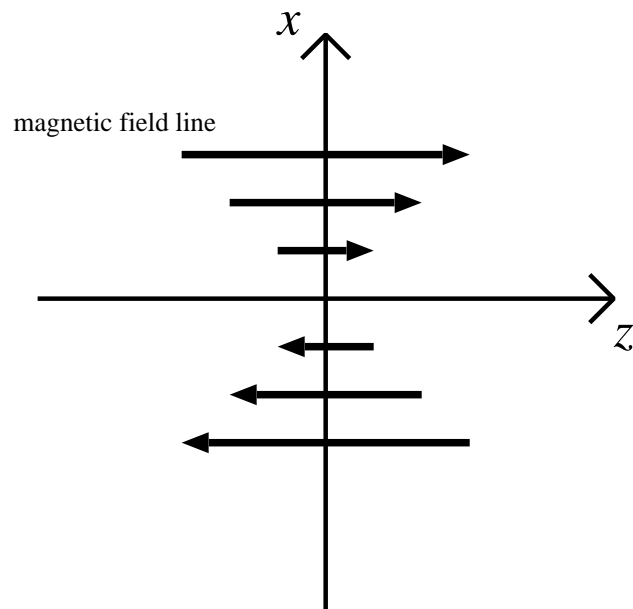
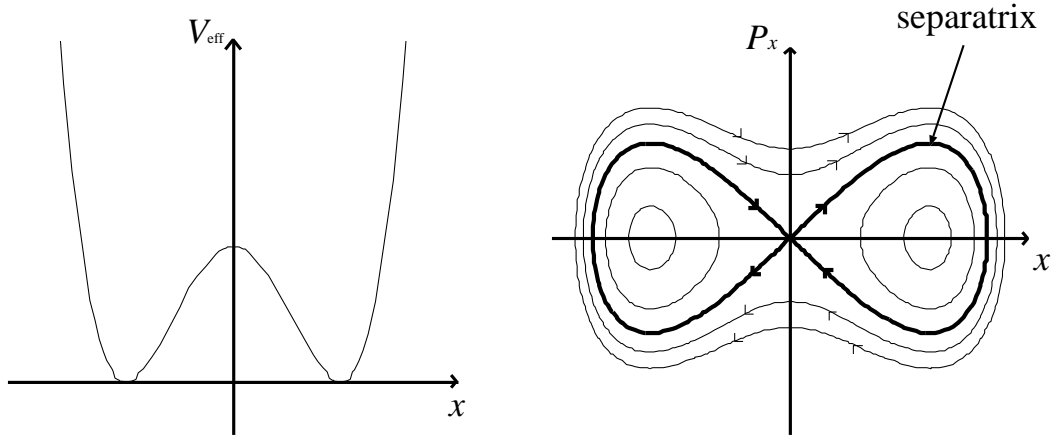Figure 3.1: Schematic drawing of one dimensional reversed magnetic field.

Figure 3.2: Effective potential given by Eq. (3.5) and phase space structure in x-p_x plane for the case that $qP_y > 0$.
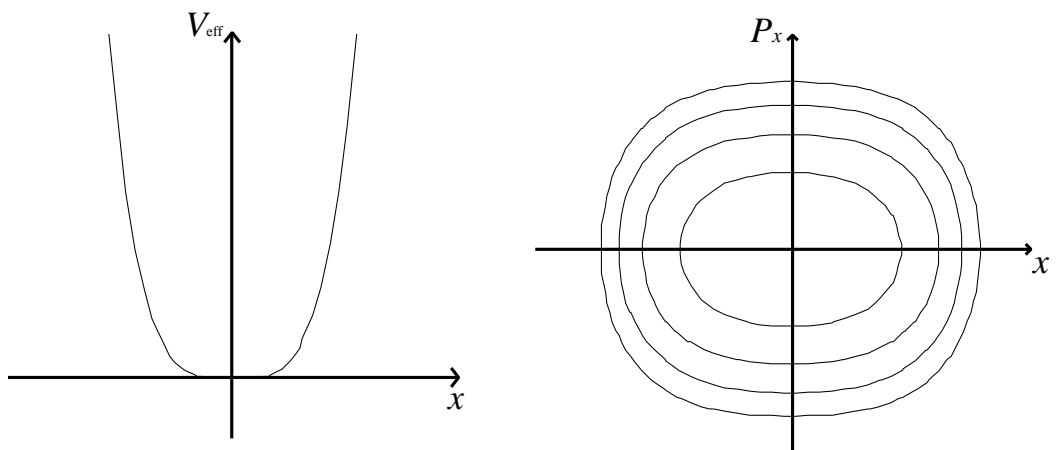

Figure 3.3: Effective potential given by Eq. (3.5) and phase space structure in x-p_x plane for the case that $qP_y < 0$.
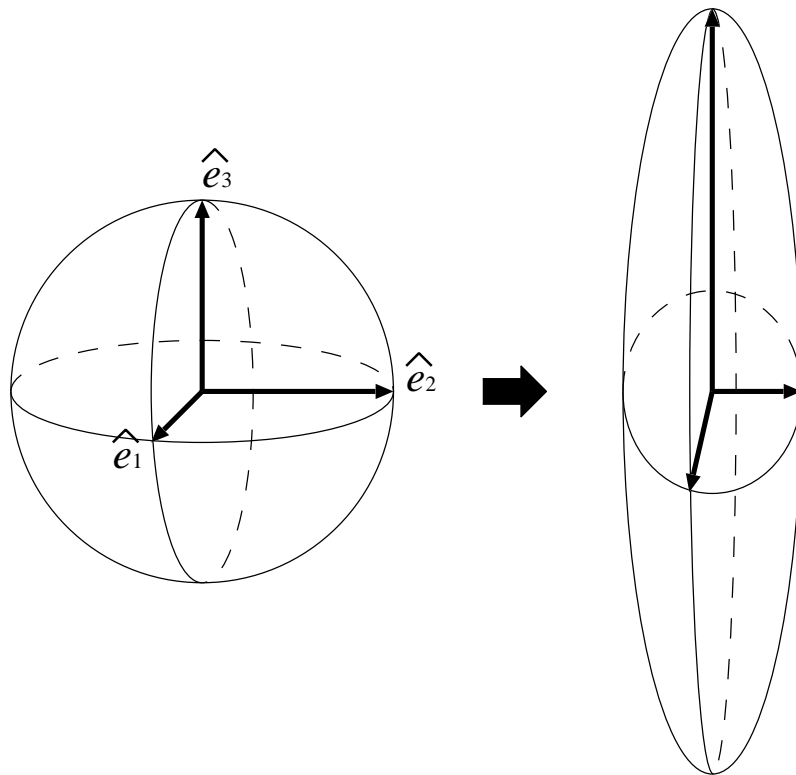
Figure 3.4: Time evolution of infinitesimal sphere spanned by the basis $\{\hat{e}_i\}$ of δx. It will be deformed into an ellipsoid.

Chapter 4

Numerical Results

4.1 Particle Trajectory and Escape Time

First, we study the motion of electron in the Y-shaped magnetic field and uniform electric field perpendicular to the magnetic field. Normalized equation (2.11) is integrated by adaptive stepsize controlled Runge-Kutta method [28]. Typical trajectories of the particle in x-y plane are shown in Figs. 4.1 and 4.2. Both trajectories are calculated with $\gamma = 1$ and the initial condition $\hat{\boldsymbol{x}} = (0.2, 0.0, 0.6)$ and $\hat{\boldsymbol{v}} = (1.0, 0.0, 1.0)$. Fig. 4.1 is for the case that $\alpha = 0.001$ and Fig. 4.2 is for $\alpha = 0.01$, which is ten times larger than the value for the Fig. 4.1. Dotted line plotted in the figures represents the neutral sheet in the region that $\hat{y} = 0$, $|\hat{x}| < \gamma$. In Fig. 4.1, the particle oscillates in y direction with bouncing in x direction because of the mirror effect. When the particle passes the bifurcation points of magnetic field at $\hat{x} = \pm\gamma$, it stochastically decides to go upward or downward. This is the orbital instability. During this motion, the particle is accelerated by the electric field in the dissipation region because it can not be magnetized in weak magnetic field region, and it drifts with $\boldsymbol{E} \times \boldsymbol{B}$ drift velocity in strong magnetic field region outside the dissipation region. In Fig. 4.2, the particle initially exhibit the same motion as the particle in Fig. 4.1, and then go out from the dissipation region after a certain time, and transfers to the phase in which it exhibits periodic bounce motion. Both particles transfers its phase from chaotic to regular phase, but the time of staying in the initial phase is different. The electric field affects on this transition time. In Fig. 4.3, we show the time series of $\hat{x}$ with the same parameters as the Fig. 4.2. We define the "escape time": T_{escape} by the time when particle never enters the dissipation region. For example, $T_{escape} = 165$ in the case of Fig. 4.3. Because T_{escape} differs between the case for different initial conditions, it is estimated by averaging over the values of ten different

initial conditions. In Fig. 4.4, average escape time against normalized electric fields are plotted. The average escape time shows power to the minus one dependence on α, $T_{escape} \sim \alpha^{-1}$. This is because the escape time is determined by the $\boldsymbol{E} \times \boldsymbol{B}$ drift velocity.

4.2 Lyapunov Exponents

Next, we calculate Lyapunov exponents to judge whether the trajectory is chaotic or not. The existence of at least one positive Lyapunov exponent means the trajectory is chaotic. Examples of calculated Lyapunov spectrums are shown in Figs. 4.5 and 4.6 with the same parameters as Figs. 4.1 and 4.2. In the Fig. 4.1, particle moves both in magnetized and unmagnetized regions and exhibit both regular and chaotic motions. This is the reason why the maximum Lyapunov exponent do not settle into some values. However, there is positive Lyapunov exponent in the Fig. 4.5, that is, we can say that the system is chaotic. In Fig. 4.6, the phase is transfered to the regular one after the escape time passed, and the maximum Lyapunov exponent gradually decreases with time and becomes close to zero. In Figs. 4.7 and 4.8, we show the sum of Lyapunov exponents for the cases of Fig. 4.5 and 4.6. The sum of Lyapunov exponents is equivalent to the Jacobian of the set of differential equations. Because the Hamiltonian does not depends on t explicitly in this system, the sum of Lyapunov exponents is zero. In the figures, the sum of Lyapunov exponents is extremely small relative to each maximum Lyapunov exponent, thus we can suppose the preciseness of the simulation is hold.

In Figs. 4.9 and 4.10, we plot the dependence of the maximum Lyapunov exponent on γ. Each figure corresponds to the case that $\alpha = 0.001$ and $\alpha = 0.01$, respectively. Both figures show that the maximum Lyapunov exponents

have a tendency to increase with decreasing γ. This result agrees with the description that the particle is scattered effectively when passing through the magnetic field bifurcation point at $x = \pm\gamma$.

The maximum Lyapunov exponents are estimated to the order 10^{-1}. The Lyapunov exponents are the mean divergence rate of nearby trajectories and then, the reciprocal of the maximum Lyapunov exponents are considered as a decorrelation time. This decorrelation time scale becomes the order 10 in normalized unit.

4.3   Velocity Distribution

We have studied the characteristic of the particle motion in the given field. However, there is a broad gap between the microscopic and macroscopic quantities. To explain macroscopic phenomena, we have to switch to the way of statistical mechanics. In a chaotic system, the principle of a priori distribution must be examined by direct simulations. So, we consider many particle dynamics which all having the same equation of motion but different initial conditions. If the velocity distribution relaxes to the Gaussian distribution, the principle of weight probability is considered to be hold.

First, we set total number of the particles 10^3, initial velocity distribution uniform between $\hat{v} = -0.5$ and $\hat{v} = 0.5$ and initial position distribution also uniform between $\hat{x} = -1.0$ and $\hat{x} = 1.0$, then examine the change of velocity distribution in three directions. In Figs. 4.11 to 4.16, we plot time evolution of velocity distributions and standard deviations of the velocity distributions in each direction. In Figs. 4.11, 4.13, 4.15, the parameters are set $\alpha = 0.005$ and $\gamma = 1$. Initial distribution, distributions at time $\hat{t} = 100$, $\hat{t} = 200$ and Gaussian fitting curve are plotted together. After the decorrelation time passed, the

26

almost Gaussian distribution is realized. For the realized velocity distribution, we define the ensemble average of quantity A

$$\bar{A} = \frac{1}{N}\sum_{i=1}^{N}\delta(v-v_i)A(v_i) \tag{4.1}$$

$$N = \sum_{i=1}^{N}\delta(v-v_i) \tag{4.2}$$

where δ is the Dirac delta.

In Figs. 4.12, 4.14, 4.16, we plot the time evolution of standard deviation of the velocity distribution for $\alpha = 0.005$ and $\gamma = 1$, 2, 5. The standard deviations linearly increase with time until the escape time. Until the escape time, unceasing heating in all the directions induced by chaos occurs. The gradient of each line increases with γ. This results are discussed in the next section.

4.4 Effective Resistivity

We see in the Fig. 4.15 that the velocity distribution in z direction shifts in positive direction, that is, average velocity in z direction is not equal to zero. This is because unmagnetized particle is accelerated by the electric field in the dissipation region, while particle only $\boldsymbol{E} \times \boldsymbol{B}$ drifts in magnetized region. The ensemble averaged velocity in z direction for $\alpha = 0.001, \gamma = 1$ is plotted in Fig. 4.17. Although the average velocity perturbes by statistical error, we can see the tendency that it initially increases, then saturate after a certain time. This saturation mechanism can be regarded as the effective collision by the chaos. According to the analogy to the friction force, the average velocity becomes proportional to the function,

$$\bar{v} \propto 1 - \exp(-\frac{\hat{t}}{T_r}), \tag{4.3}$$

27

where T_r is a relaxation time. So, we estimate the effective collision frequency $\nu_{\text{eff}} \equiv 1/T_r$ by fitting with the function. Dependence of effective collision frequency on normalized electric field is summarized in Table. 4.1.

Table 4.1: Dependence of relaxation time and effective collision frequency on normalized electric field ($\gamma = 1$).

α	0.001	0.002	0.005	0.01
T_r	178.7	121.6	35.79	22.08
$\nu_{\text{eff}}[\times 10^7/s]$	0.982	1.44	4.90	7.95

We can derive the effective resistivity by two way from the results of the average velocity in z direction. First, we use the saturated average velocity $\bar{v}_\infty$. Current is given by the following equation,

$$j = en\bar{v}_\infty, \tag{4.4}$$

where n is density. We can calculate the corresponding effective resistivity from the Ohm's law,

$$\eta_1 = \frac{E}{j} = \frac{1}{en}\frac{E}{\bar{v}_\infty}. \tag{4.5}$$

The second way to estimate effective resistivity uses the effective collision frequency, which is a relaxation time scale of momentum. The averaged collective motion of particles in z direction can be represented as follows,

$$m\frac{d\bar{v}}{dt} = qE - m\nu_{\text{eff}}\bar{v}. \tag{4.6}$$

The effect of magnetic field is supposed something like friction force represented by the second term in Eq. (4.6). Solving this equation yields

$$\bar{v} = \frac{qE}{m\nu_{\text{eff}}}(1 - \exp(-\nu_{\text{eff}}t)). \tag{4.7}$$

This gives the relation between ν_{eff} and $\bar{v}_\infty$, that is,

$$\bar{v}_\infty = \frac{qE}{m\nu_{eff}}. \tag{4.8}$$

Using this saturated average velocity and Ohm's law, we obtain another formula of resistivity,

$$\eta_2 = \frac{m\nu_{\text{eff}}}{ne^2}. \tag{4.9}$$

This is an usual derivation of resistivity. By using these two formulas, we estimate the effective resistivity induced by chaotic motion of electrons. Because n is arbitrary, we plot the effective resistivity calculated by both equations times n against α in Fig. 4.18. η_1 is larger than η_2 by a factor one to three. This means the relation (4.8) is violated. We conclude that while in single particle dynamics the relation (4.8) holds, effective mass or charge of the collective of particles are different from a single particle or the way of acting the electric field on the collective of particles are different from it on a single particle and the relation is violated in this system. This is the collective effect of chaotic system. In Fig. 4.17, we also plot the line which represents free acceleration of a single particle by the electric field without magnetic field. The fact that the gradient of the numerical result is smaller than that of the free acceleration proves that the difference between the single particle dynamics and the collective dynamics.

In Fig. 4.19, dependence of saturated average velocity on γ is shown. The figure shows that saturated velocity increases with γ, that is, the resistivity decreases with increasing γ. This results again agree with the description that γ weakens the chaotic effect. Now, we go back to the results of Sec. 4.3. We explain well the results that the collective of particles is more rapidly heated in the case that γ is larger by Ohmic heating induced by this effective resistivity. Ohmic heating rate represented by ηj^2 is propotional to $\bar{v}_\infty$ because $j \propto \bar{v}_\infty$ and

29

$\eta \propto \bar{v}_\infty^{-1}$. Thus, we conclude that if the Ohmic heating occurs by the effective resistivity induced by chaos, the larger γ becomes, the more effectively the collective particles is heated.
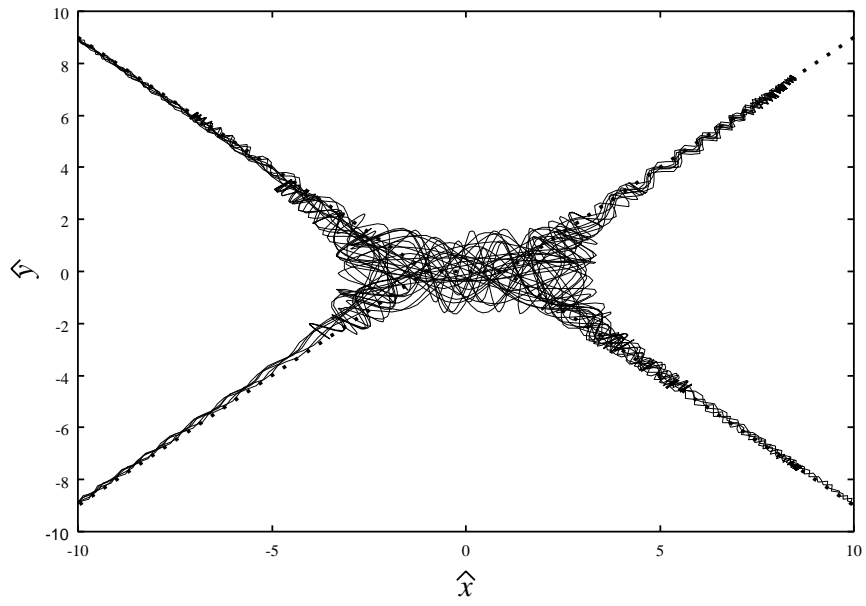
Figure 4.1: Typical orbit in x-y plane for $\alpha = 0.001$. Particle moves in a weak magnetic field region.
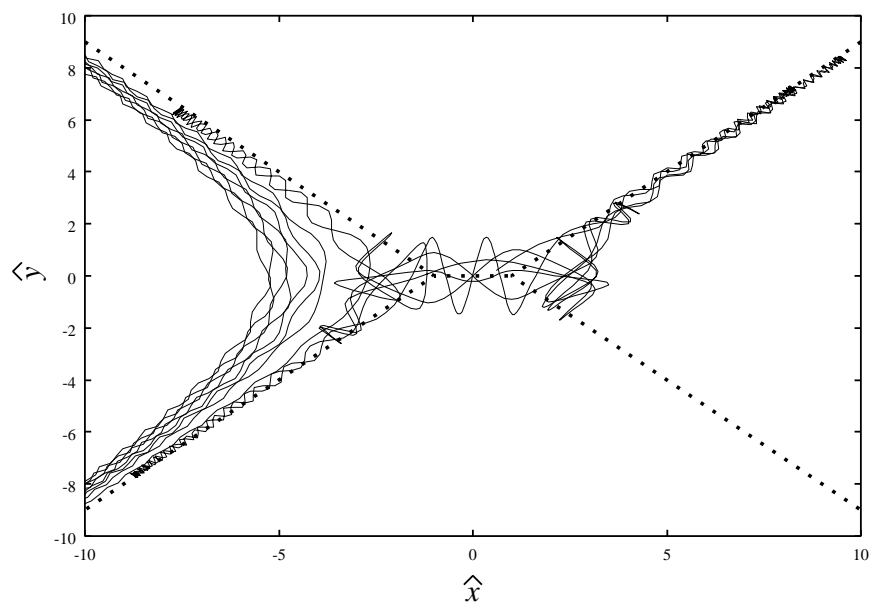
Figure 4.2: Typical orbit in x-y plane for $\alpha = 0.01$. Particle initially moves in a weak magnetic field region, then go out to the left hand side, which is a strong magnetic field region.
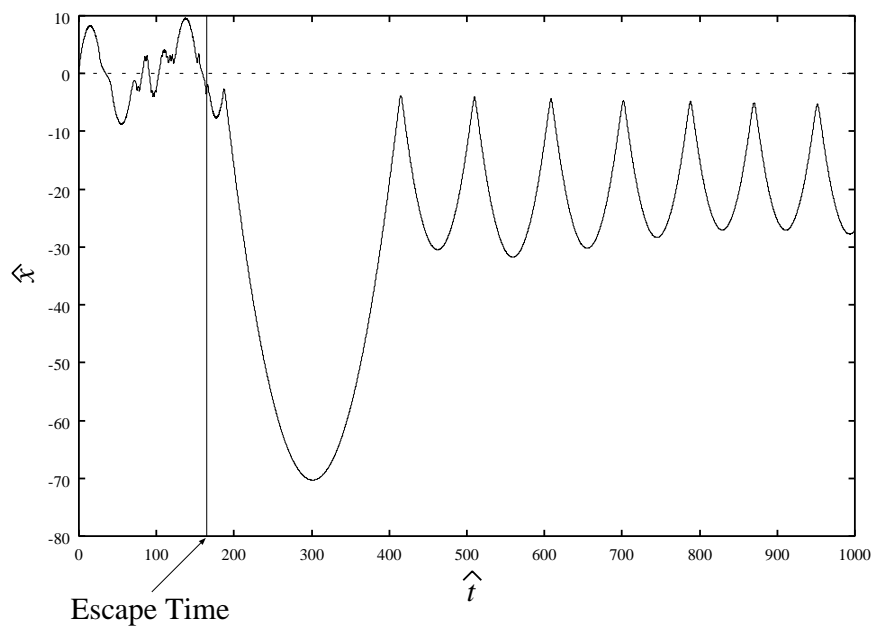
Figure 4.3: Solid line shows time series of $\hat{x}$. After T_{escape}, particle never crosses the $\hat{x} = 0$ line.
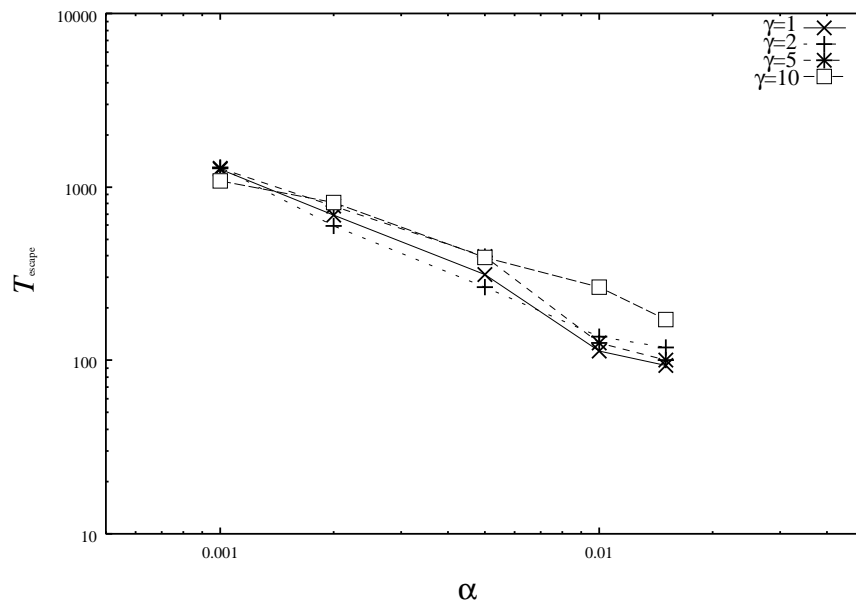
Figure 4.4: Dependence of escape time T_{escape} on α and γ. T_{escape} shows the power to minus one dependence on α.
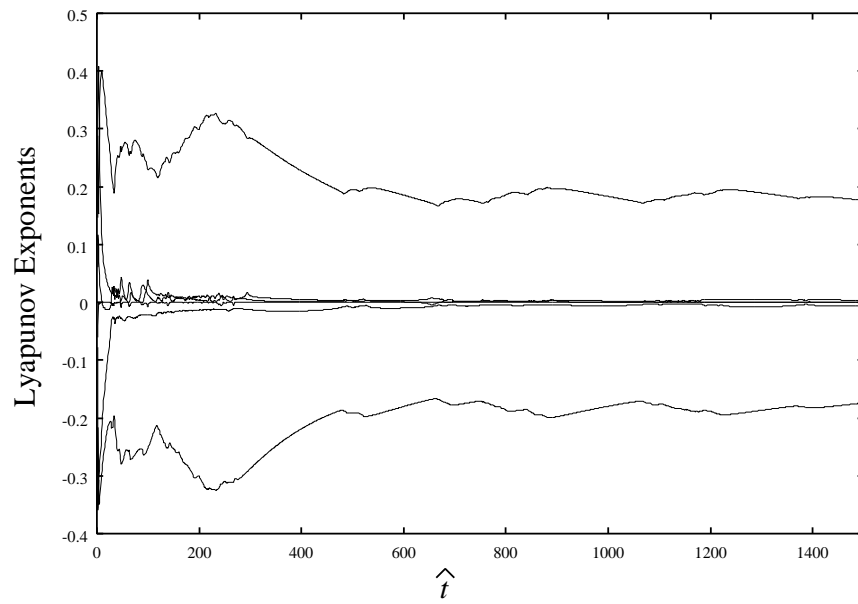
Figure 4.5: Lyapunov spectrum for $\alpha = 0.001$.
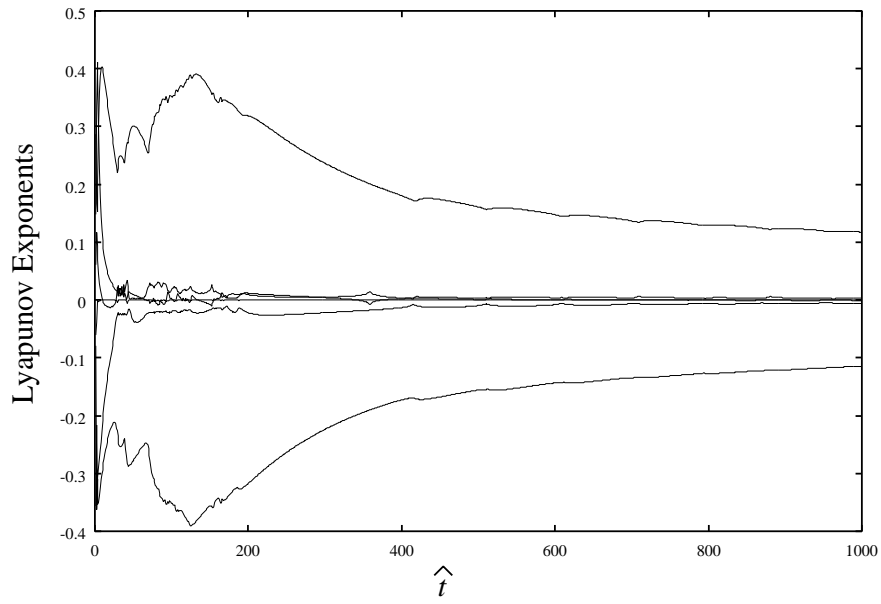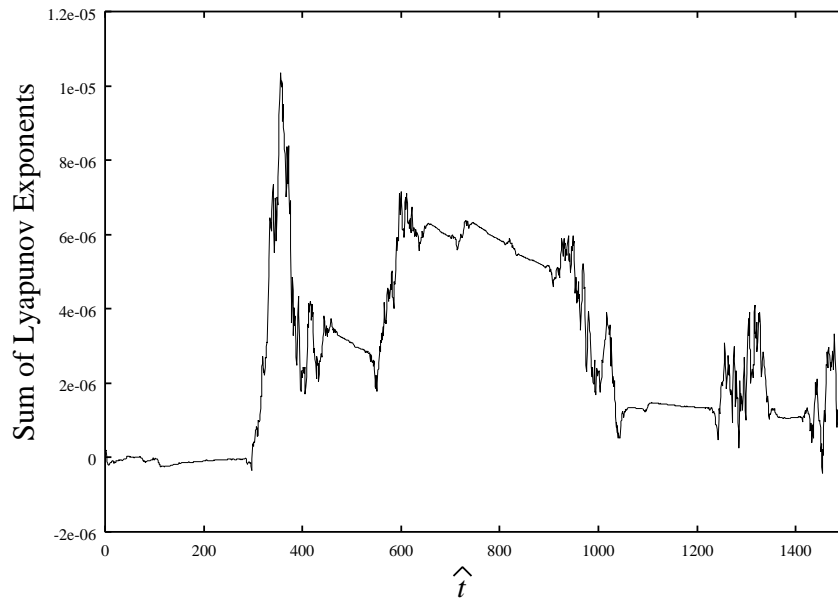
Figure 4.6: Lyapunov spectrum for $\alpha = 0.01$.

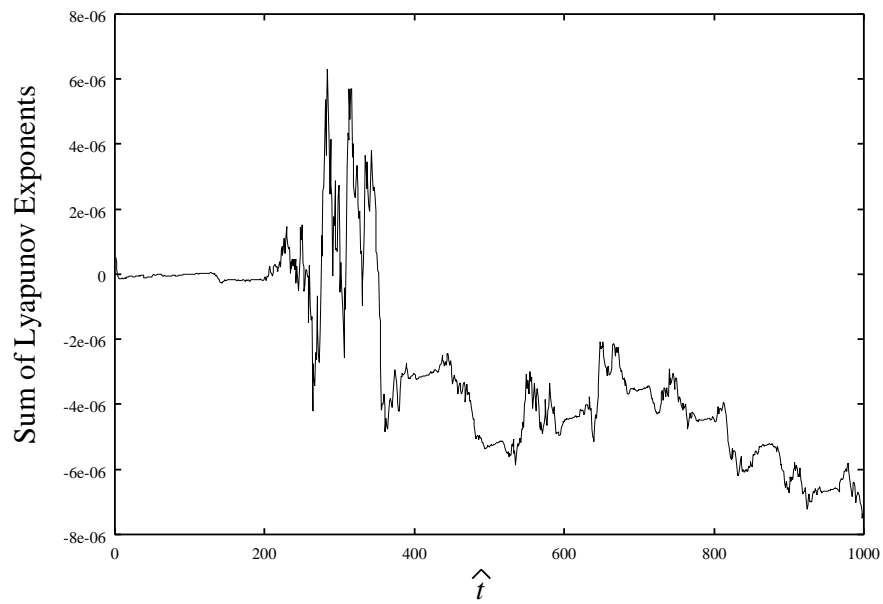Figure 4.7: Sum of Lyapunov Exponents for $\alpha = 0.001$.

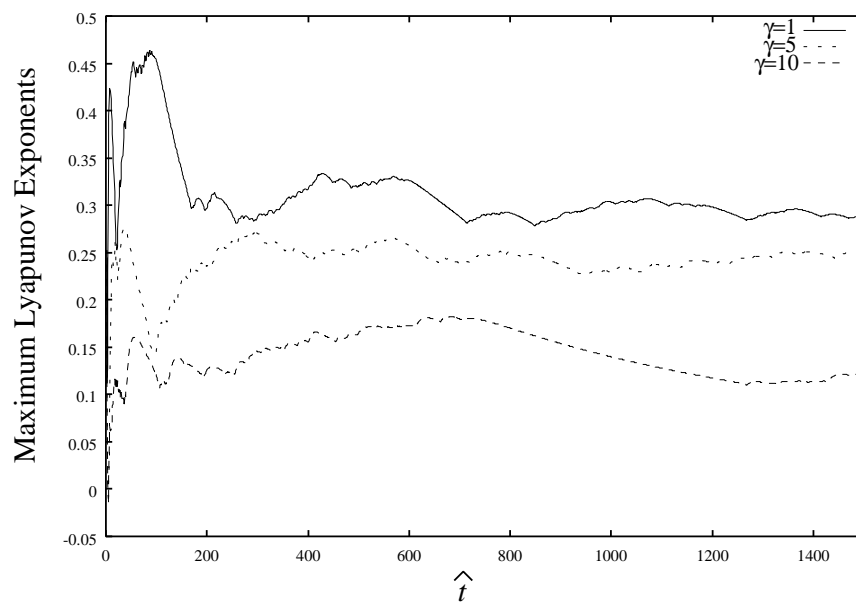Figure 4.8: Sum of Lyapunov exponents for $\alpha = 0.01$.

Figure 4.9: Dependence of maximum Lyapunov exponents on γ for the case $\alpha = 0.001$.
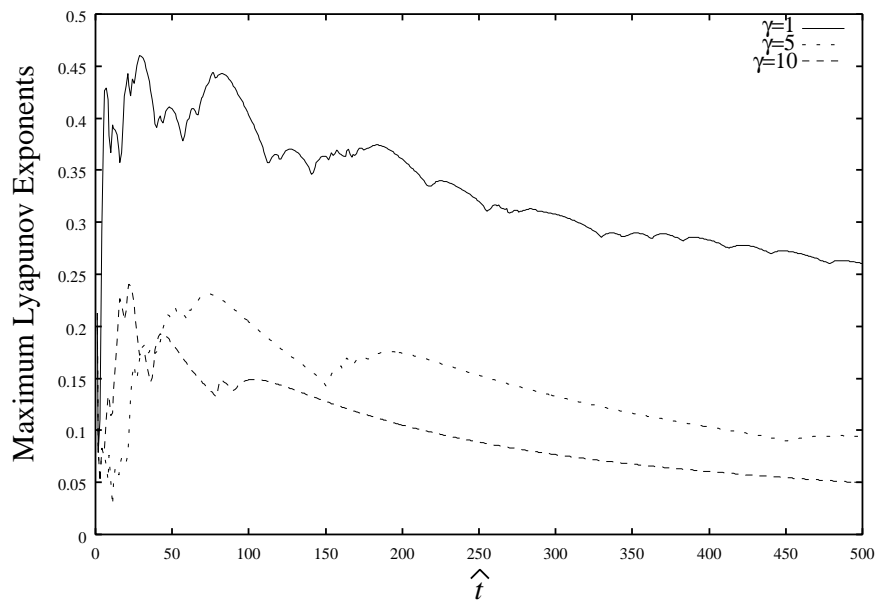
Figure 4.10: Dependence of maximum Lyapunov exponents on γ for the case $\alpha = 0.01$.
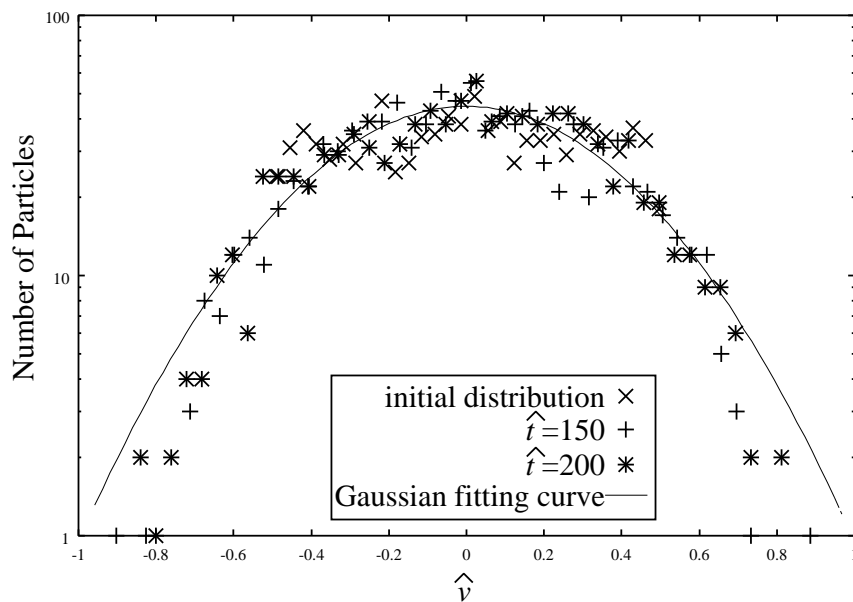

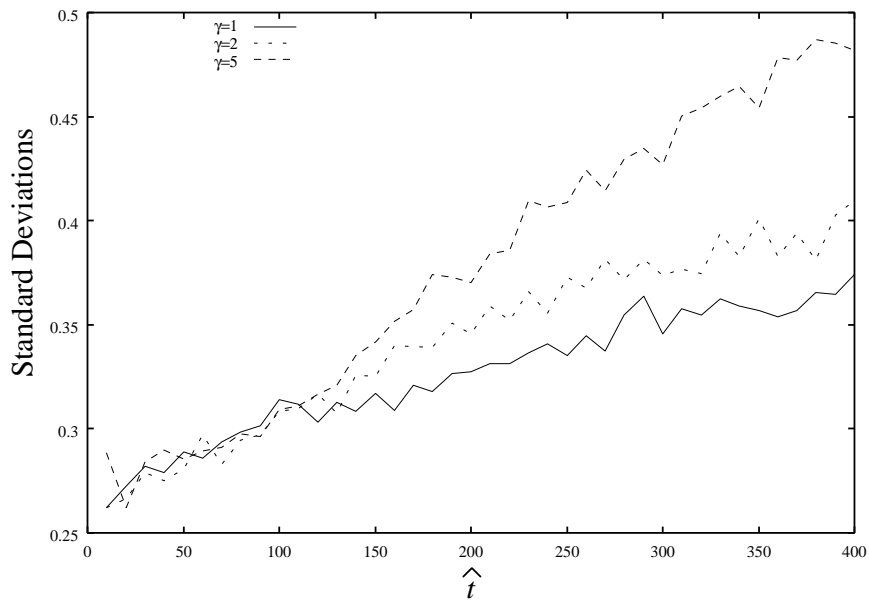Figure 4.11: Time evolution of velocity distribution in x direction.

Figure 4.12: Time evolution of standard deviations of the velocity distribution in x direction. The results for different γ are plotted.

Figure 4.13: Time evolution of velocity distribution in y direction.

Figure 4.14: Time evolution of standard deviations of the velocity distribution in y direction. The results for different γ are plotted.
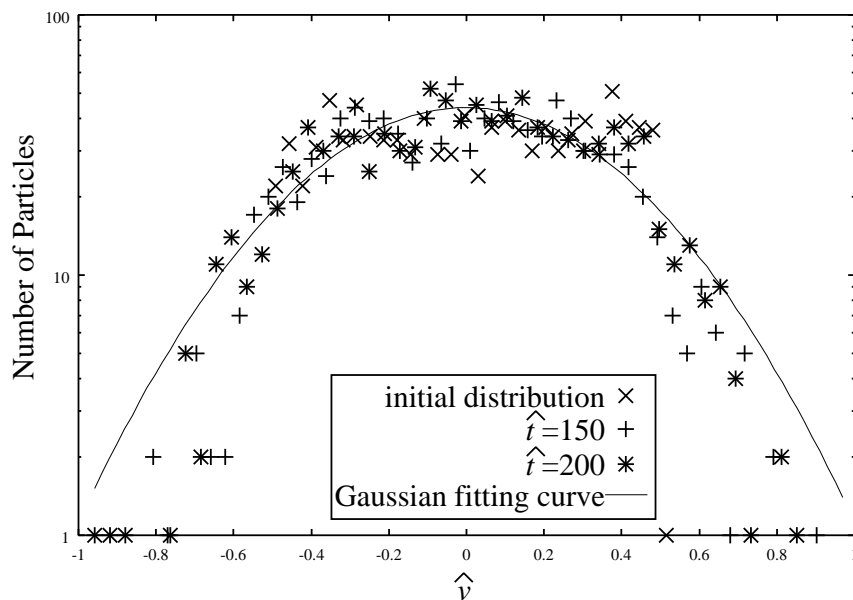

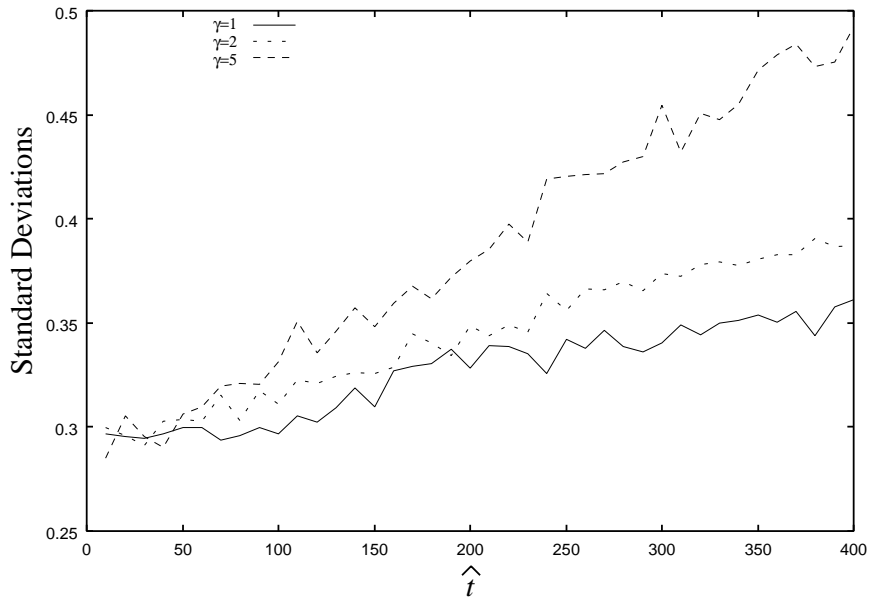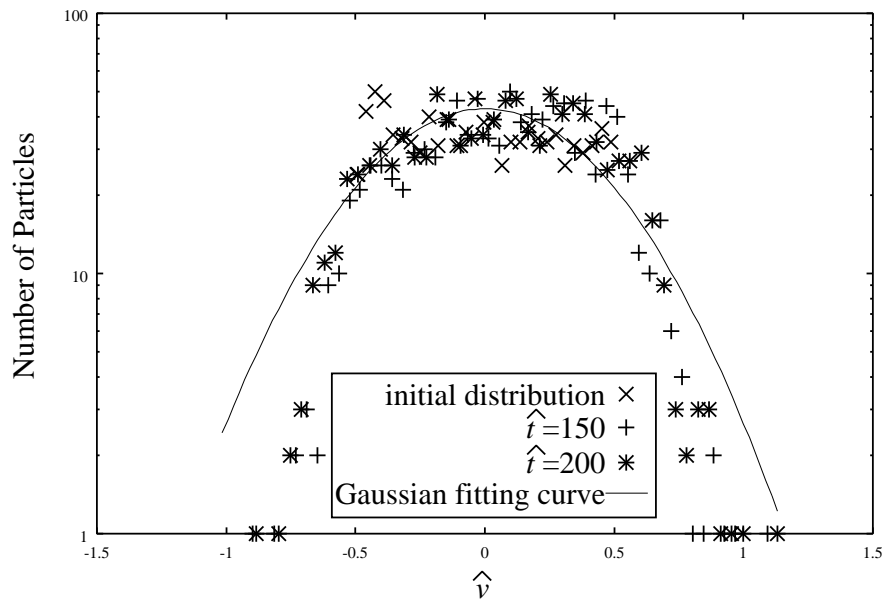Figure 4.15: Time evolution of velocity distribution in z direction.
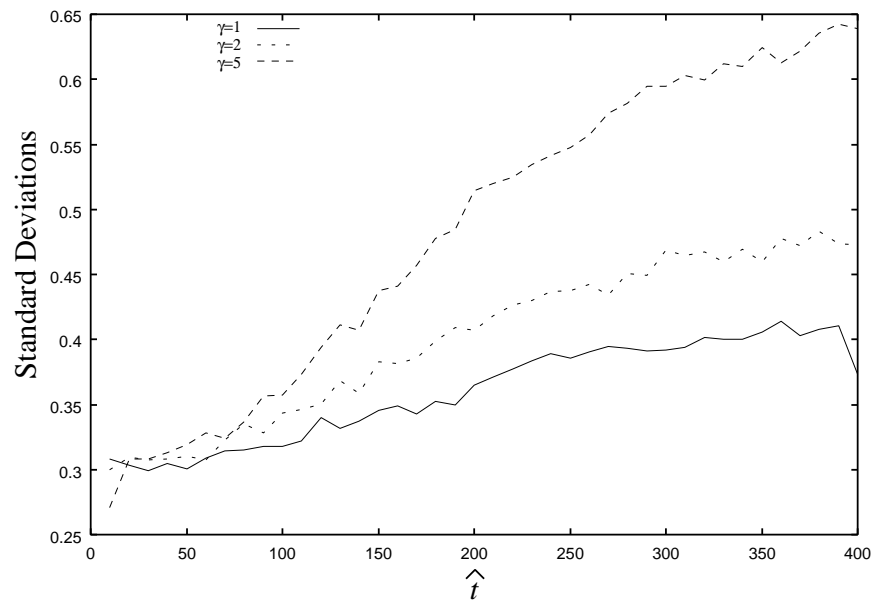
Figure 4.16: Time evolution of standard deviations of the velocity distribution in z direction. The results for different γ are plotted.
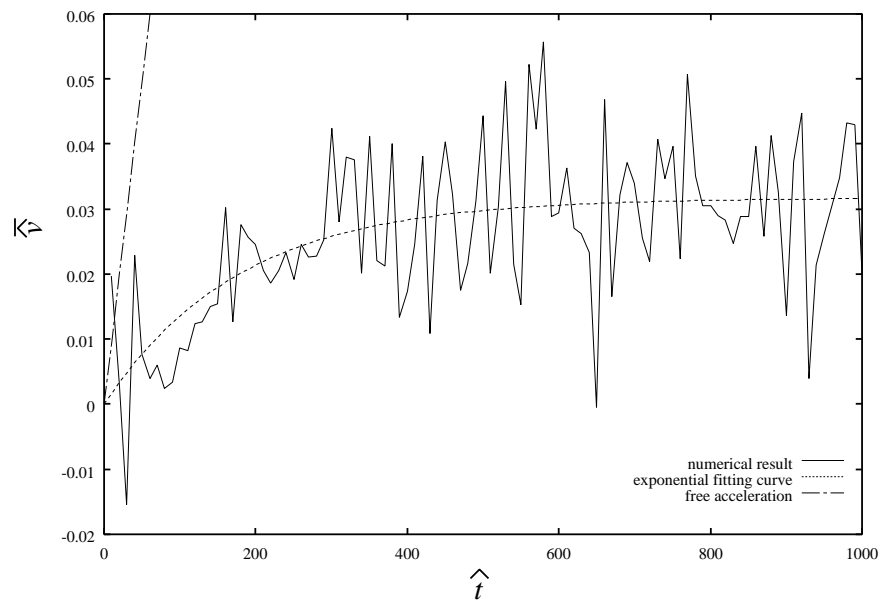
Figure 4.17: Time series of averaged velocity in z direction for $\alpha = 0.001$ and $\gamma = 1$. Broken line represents free acceleration of single particle by the electric field without magnetic field. Collective of particles is less accelerated than single particle.

Figure 4.18: Effective resistivity times density against normalized electric field α. η_1 and η_2 differ by a factor.

Figure 4.19: Dependence of saturated normalized velocity in z direction on γ.

Chapter 5

Discussion and Summary

We have studied microscopic chaos of particle trajectories, then statistical properties of the chaotic motion of charged particle in the Y-shaped model configuration and estimated the effective resistivity induced by chaotic motion. The velocity distributions i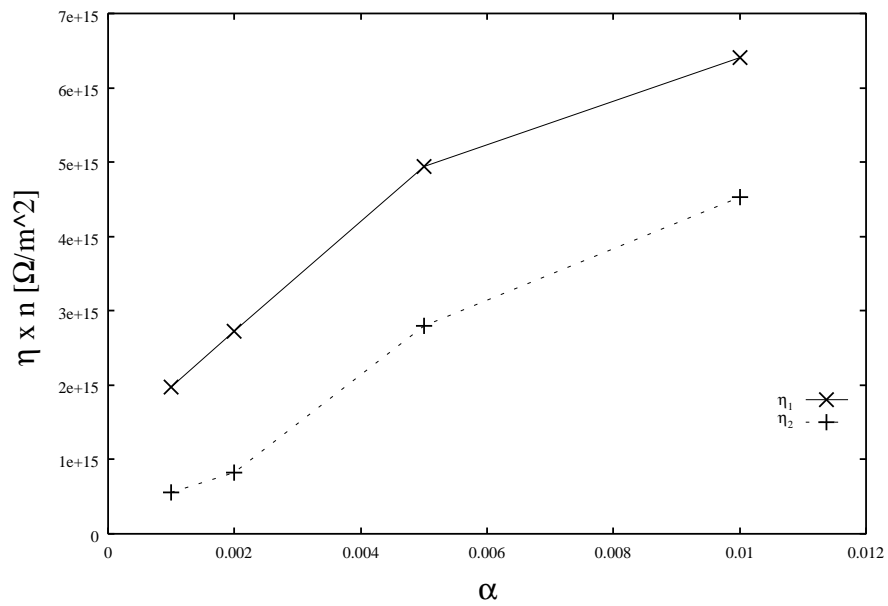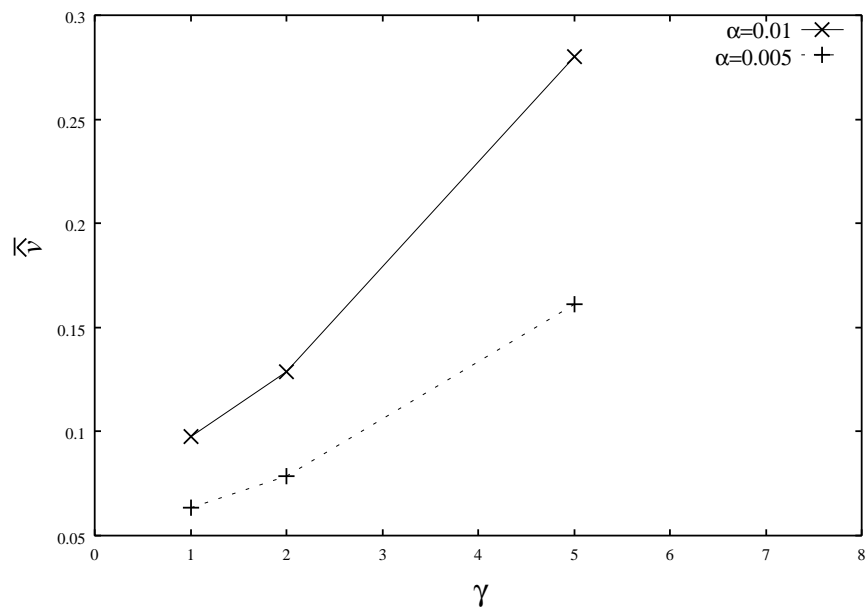n all direction relax to the Gaussian distribution after a Lyapunov decorrelation time scale. By using the realized velocity distribution, we define the ensemble average,

$$\bar{A} = \frac{1}{N} \sum_i A(v_i) f(v_i). \tag{5.1}$$

We note that the distribution in the direction along the electric field (z direction) is shifted and finite average velocity exists in z direction. However, particles are less accelerated than free acceleration by the electric field without magnetic field and the averaged velocity saturate after certain time. This fact suggests the existence of collision like mechanism which produces resistivity. We estimate the resistivity by using two formulas, one uses saturated average velocity and the other uses the effective collision frequency. These effective resistivity differ by a factor, which means that the relation between $\bar{v}_\infty$ and ν_{eff}, given by the Eq. (4.8), is violated. This is because the effective collision mechanism induced by chaotic motion of particles is essentially different from usual collision. We consider that effective mass or charge or electric field is different from the case of single particle dynamics. This is reflected to the result that collective particles is less accelerated by the electric field shown in Fig. 4.17.

Here, we compare the derived effective resistivity to conventional Spitzer resistivity. Spitzer calculated resistivity with taking into account the ion recoil in each collision and being averaged over the electron distribution. The following equation is Spitzer resistivity for hydrogen [29],

$$\eta_{\text{Spitzer}} = 5.2 \times 10^{-5} \frac{Z \ln \Lambda}{T_e^{\frac{3}{2}} [\text{eV}]} [\Omega \cdot m], \tag{5.2}$$

where Z is the ion charge number, T is plasma temperature and Λ is the maximum impact parameter. Because the effective resistivity which we derived as $\eta \propto 10^{15}/n$ depends only on plasma density and Spitzer resistivity is proportional to $T^{-\frac{3}{2}}$, the effective resistivity becomes dominant relative to the collisional resistivity in high temperature rarefied plasmas. Comparison between Spitzer resistivity set $Z = 1$ and $\ln \Lambda = 10$ and the effective resistivity for various situations are plotted in Fig. 5.1. We summarize typical parameters in each situation in Table. 5.1. For example, in solar corona, the effective

Table 5.1: Typical values of density and temperature in various situations.

	Density n $[m^{-3}]$	Temperature T [eV]
Solar Corona	10^{15}	10^2
Magnetoshpere	10^6	10^2
Fusion Plasma	10^{21}	10^4

resistivity is about 10^6 times larger than the Spitzer resistivity at $T = 100$ [eV].

Finally, we discuss the effect of the plasma flow by the $\boldsymbol{E} \times \boldsymbol{B}$ drift. The $\boldsymbol{E} \times \boldsymbol{B}$ drift provides the inflow in y direction and outflow in x direction to the dissipation region. Because of this flow, low energy particles penetrate into the dissipation region and absorb the magnetic energy, then go out from the region. Thus, steady exchange of energy from magnetic field energy to kinetic energy occurs. By taking the MHD effect into consideration, the conservation of the particles leads the plasma density in the dissipation region.
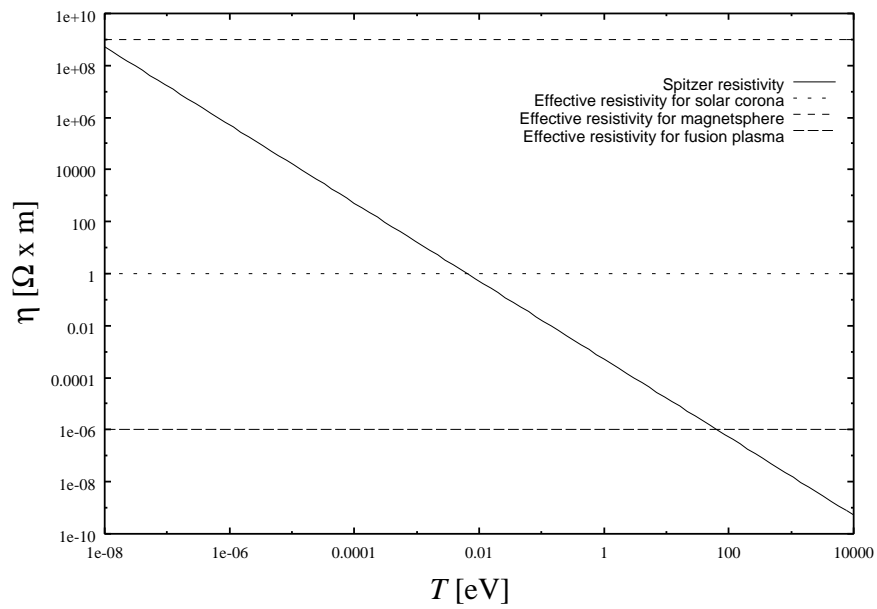
Figure 5.1: Comparison between the Spitzer resistivity and the effective resistivity for various situations.

We summarize the obtained results about the chaos induced collision-less resistivity in the magnetic reconnection like Y-shaped model field.

- In the proposed magnetic field, the charged particle exhibits the chaotic motion.

- The global time scale of the motion is determined by the escape time scale from the dissipation region. In this time scale, effective collision induced by chaos occurs, which is a different mechanism from usual collision in the sense that effective force acting on collective particles differs from that on a single particle and the collective particles is less accelerated than single particle.

- The effective resistivity is estimated as $\eta \sim 10^{15}/n$ $[\Omega \cdot m]$. Since the effective resistivity depends on plasma density and does not depend on plasma temperature, it becomes more dominant than collisional Spitzer resistivity in rarefied and high temperature plasmas.

- Dependence of the effective resistivity on the parameters are studied. The intensity of the transverse electric α field enlarges the resistivity, while the length in x direction γ weakens the chaotic effects and the resistivity. However, the Ohmic heating by the effective resistivity increases with γ.

Appendix A

Harris-Sheet

In section 2.1, we proposed Y-shaped magnetic field configuration to analyze the particle dynamics in a reconnection process. This configuration has a great similarity to well known Harris-type configuration (hereafter, it is refered to Harris-Sheet)[30]. Here we give a brief view of Harris-Sheet.

The Harris-Sheet is one of the exact steady-state solution of the Vlasov-Maxwell equations. The equations to be solved are

$$\boldsymbol{v} \cdot \frac{\partial f}{\partial \boldsymbol{r}} + \frac{q}{m}(\boldsymbol{E} + \boldsymbol{v} \times \boldsymbol{B}) \cdot \frac{\partial f}{\partial \boldsymbol{v}} = 0 \tag{A.1}$$

$$\nabla \cdot \boldsymbol{E} = \frac{1}{\epsilon_0} \sum q \int f d\boldsymbol{v} \tag{A.2}$$

$$\nabla \times \boldsymbol{B} = \mu_0 \sum q \int f\boldsymbol{v} d\boldsymbol{v}. \tag{A.3}$$

where q and m are the appropriate values for ions and electrons. The summation must be taken over species of particles (ions and electrons) with appropriate q and f.

If we consider $\boldsymbol{E}, \boldsymbol{B}$ and f which depend only on one coordinate (say x coordinate), then we know that the energy and the momenta conjugate to y and z are constants of the motion. These are

$$W = \frac{1}{2}m(v_x^2 + v_y^2 + v_z^2) + q\phi(x), \tag{A.4}$$

50

$$p_y = mv_y + qA_y(x), \tag{A.5}$$

$$p_z = mv_z + qA_z(x), \tag{A.6}$$

where $\boldsymbol{A}(x)$ is the vector potential. We assume that $\boldsymbol{E}$ and $\boldsymbol{B}$ has only an x and z componet,respectively. Then $\boldsymbol{A}$ may be taken to have only a y component. It is convenient to rearrange equations (A.4),(A.5) and (A.6) to give the constants of motion

$$\alpha_1^2 = v_x^2 - \frac{2q}{m}v_yA_y - \frac{q^2}{m^2}A_y^2 + \frac{2q}{m}\phi, \tag{A.7}$$

$$\alpha_2 = v_y + \frac{q}{m}A_y, \tag{A.8}$$

$$\alpha_3 = v_z. \tag{A.9}$$

There is a set $(\alpha_1, \alpha_2, \alpha_3)$ for the ions and electrons. The solution of equation (A.1) is $f = f(\alpha_1, \alpha_2, \alpha_3)$. Substituting this into equations (A.2) and (A.3) gives two coupled differential equations for ϕ and A_y. The nature of the solution will depend on our choice of f and the boundary conditions.

We will assume that at $x = 0$ the distribution functions are Maxwellian centered about some mean velocity in the y direction.

$$f_{i,e} = (\frac{m_{i,e}}{2\pi T})^{\frac{3}{2}} N \exp[-\frac{m_{i,e}}{2T}\{\alpha_1^2 + (\alpha_2 - V_{i,e}) + \alpha_3^2\}], \tag{A.10}$$

where subscript i and e correspond to ions and electrons and V is the mean velocity. If we transform the coordinate system on which the relation $V_e = -V_i = -V$ is satisfied and then substitute equation (A.10) into equations (A.2) and (A.3) the following equations for the potentials ϕ and A_y are obtained

$$\frac{d^2\phi}{dx^2} = -\frac{qN}{\epsilon_0}\exp(\frac{q}{T}VA_y)[\exp(-\frac{q}{T}\phi) - \exp(\frac{q}{T}\phi)] \tag{A.11}$$

$$\frac{d^2A_y}{dx^2} = -\mu_0qNV\exp(\frac{q}{T}VA_y)[\exp(-\frac{q}{T}\phi) + \exp(\frac{q}{T}\phi)] \tag{A.12}$$

$$\tag{A.13}$$

Equation (A.11) is clearly satisfied by $\phi = 0$. Then equation (A.12) becomes

$$\frac{dA_y^2}{dx^2} = -2\mu_0 qNV \exp(\frac{q}{T}VA_y) \tag{A.14}$$

If the boundary conditions are taken to be $A_y = 0$ and $B = 0$ at $x = 0$, the solution of equation (A.14) is

$$A_y = \frac{2T}{qV} \log \cosh(\frac{Vx}{cL_D}), \tag{A.15}$$

where $L_D = (\frac{\epsilon_0 T}{Nq^2})^{\frac{1}{2}}$ is the Debye length. From which we find the magnetic field

$$B = -2\sqrt{\mu_0 TN} \tanh(\sqrt{\frac{\mu_0 N}{T}}qVx). \tag{A.16}$$

From equation (A.11), we can find easily that the ion and electron densities are given by

$$n_{i,e} = N \exp(\frac{qV}{T}A_y), \tag{A.17}$$

which, when combined with equation (A.15) gives

$$n_{i,e} = \frac{N}{\cosh(\frac{Vx}{cL_D})}. \tag{A.18}$$

Fig. A.1 gives the variation of B and n across the sheath which shows the balance of magnetic pressure and plasma pressure.
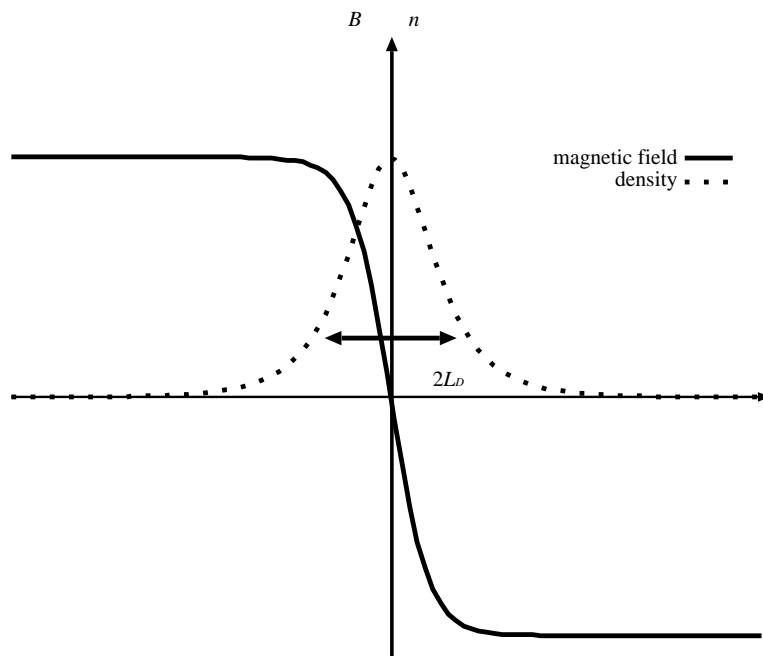
Figure A.1: The magnetic field and density profile in a Harris-Sheet.

References

[1] R. M. Kulsrud, Phys. Plasmas **5**, 1599 (1998)

[2] T. Tajima, K. Shibata, *Plasma Astrophysics* (Addison-Wesley, Massachusetts, 1997)

[3] D. Biskamp, *Nonlinear Magnetohydrodynamics* (Cambridge University Press, Cambridge, 1993)

[4] H. E. Petschek, *Physics of Solar Flares*, NASA Sp-50 (National Aeronautics and Space Administration, Washington, 1964)

[5] G. E. Vekstein, E. R. Priest, Phys. Plasmas **2**, 3169 (1995)

[6] R. A. Treumann, W. Baumjohann, *Advanced Space Plasma Physics* (Imperial College Press, London, 1997)

[7] T. W. Speiser, J. Geophys. Res. **70**, 4219 (1965)

[8] T. W. Speiser, Planet Space Sci. **18**, 613 (1970)

[9] L. W. Lyons, T. W. Speiser, J. Geophys. Res. **90**, 8543 (1985)

[10] Z. Yoshida, H. Asakura, H. Kakuno, J. Morikawa, K. Takemura, S. Takizawa, T. Uchida, Phys. Rev. Lett. **81**, 2458 (1998)

[11] Z. Yoshida, T. Uchida, Jpn. J. Appl. Phys. **34**, 4213 (1995)

[12] A. J. Lichtenberg, M. A. Lieberman, *Regular and Stochastic Motion* (Springer-Verlag, New York, 1983)

[13] Z. Yoshida, *Introduction to Nonlinear Sciences* (Iwanamishoten, Tokyo, 1998) (In Japanese)

[14] W. Horton, Y-H Ichikawa, *Chaos and Structures in Nonlinear Plasmas* (World Scientific, Singapore, 1996)

[15] H. Asakura, K. Takemura, Z. Yoshida, T. Uchida, Jpn. J. Appl. Phys. **36**, 4493 (1997)

[16] W. Horton, C. Liu, B. Burns, T. Tajima, Phys. Fluids **B 3**, 2192 (1991)

[17] W. Horton, C. Liu, J. Hernandez, T. Tajima, Geophys. Res. Lett. **18**, 1575 (1991)

[18] I. Doxas, W. Horton, K. Sandusky, T. Tajima, R. Steinolfson, J. Geophys. Res. **95**, 12033 (1990)

[19] R. Horiuchi, T. Sato, Phys. Fluids **B 2**, 2652 (1990)

[20] J. Chen, P. J. Palmadesso, J. Geophys. Res. **91**, 1499 (1986)

[21] J. Chen, H. G. Mitchell, P. J. Palmadesso, J. Geophys. Res. **95**, 15141 (1990)

[22] J. Büchner, L. M. Zelenyi, J. Geophys. Res. **92**, 13456 (1987)

[23] I. Shimada, T. Nagashima, Prog. Theo. Phys. **61**, 1605 (1979)

[24] M. Toda, R. Kubo, N. Saito, *Statistical Physics I* (Springer-Verlag, Berlin, 1991)

[25] C. Beck, F. Schlögel, *Thermodynamics of Chaotic Systems* (Cambridge University Press, Cambridge, 1993)

[26] N. G. Van Kampen, *Stochastic Processes in Physics and Chemistry* (North-Holland, Amsterdam, 1981)

[27] R. Balescu, *Statistical Dynamics* (Imperial College Press, London, 1997)

[28] W. T. Vetterling, W. H. Press, S. A. Teukolsky, B. P. Flannery, *Numerical Recipes in Fortran* (Cambridge University Press, Cambridge, 1994)

[29] F. F. Chen, *Introduction to Plasma Physics and Controlled Fusion* (Plenum Press, New York, 1974)

[30] E. G. Harris, Nuovo Cimento **23**, 117 (1962)